

The influenza NS1 protein modulates RIG-I activation via a strain-specific direct interaction with the second CARD of RIG-I.

Alexander S. Jureka<sup>1</sup>, Alex B. Kleinpeter<sup>1</sup>, Jennifer L. Tipper<sup>2</sup>, Kevin S. Harrod<sup>2</sup>, Chad M. Petit<sup>1,\*</sup>

From the <sup>1</sup>Department of Biochemistry and Molecular Genetics, University of Alabama at Birmingham School of Medicine, Birmingham, Alabama 35294, USA; <sup>2</sup>Department of Anesthesiology and Perioperative Medicine, Division of Molecular and Translational Biomedicine, University of Alabama at Birmingham School of Medicine, Birmingham, Alabama 35294, USA

Running title: Modulation of RIG-I Activation by the Influenza NS1 Protein

\*To whom correspondence should be addressed: Chad M. Petit: Department of Biochemistry and Molecular Genetics, University of Alabama at Birmingham, Birmingham, Alabama 35294; [cpetit@uab.edu](mailto:cpetit@uab.edu); Tel. (205) 975 – 3398.

**Keywords:** 1918 H1N1, RIG-I, TRIM25, non-structural protein 1, NS1, influenza, viral protein, host-pathogen interaction, infectious disease, innate immunity, nuclear magnetic resonance (NMR)

## ABSTRACT

A critical role of the influenza A virus non-structural protein 1 (NS1) is to antagonize the host cellular antiviral response. NS1 accomplishes this role through numerous interactions with host proteins including the cytoplasmic pathogen-recognition receptor, retinoic acid inducible gene I (RIG-I). Although the consequences of this interaction have been studied, the complete mechanism by which NS1 antagonizes RIG-I signaling remains unclear. We previously demonstrated that the NS1 RNA binding domain (NS1<sup>RBD</sup>) interacts directly with the second caspase activation and recruitment domain (CARD) of RIG-I. We also identified that a single strain-specific polymorphism in the NS1<sup>RBD</sup> (R21Q) completely abrogates this interaction. Here we investigate the functional consequences of an R21Q mutation on NS1's ability to antagonize RIG-I signaling. We observed that an influenza virus harboring the R21Q mutation in NS1 results in significant upregulation of RIG-I signaling. In support of this, we determined that an R21Q mutation in NS1 results in a marked deficit in NS1's ability to antagonize TRIM25-mediated ubiquitination of the RIG-I CARDS, a critical step in RIG-I activation. We also observed that wild-type NS1 is capable of binding directly to the tandem RIG-I CARDS while the R21Q mutation in NS1 significantly inhibits this interaction. Furthermore, we determined that the R21Q

mutation does not impede the interaction between NS1 and TRIM25 nor the NS1<sup>RBD</sup>'s ability to bind RNA. The data presented here offer significant insights into NS1's antagonism of RIG-I and illustrate the importance of understanding the role of strain-specific polymorphisms in the context of this specific NS1 function.

The influenza A virus (IAV) is a serious public health concern that causes annual epidemics and occasional pandemics resulting in significant levels of morbidity and mortality each year (1,2). The ability of IAV to adapt to various hosts and undergo genetic reassortment ensures constant generation of unique strains with unknown degrees of pathogenicity, transmissibility, and pandemic potential. Currently, our knowledge of the precise combination of factors that drives the emergence of strains with pandemic potential is incomplete. However, several proteins expressed by IAV have been identified as key determinants of virulence during infection. One such protein encoded by IAV is the non-structural protein 1 (NS1).

NS1 is highly multifunctional and ranges in size from 215-237 amino acids in length depending on the strain from which it is derived. During infection, NS1 plays a critical role in antagonizing the cellular innate immune response (3-5). It consists of two independently folding functional domains: the N-terminal RNA-binding

domain (NS1<sup>RBD</sup>) and the C-terminal effector domain (NS1<sup>ED</sup>). Both domains facilitate the immunosuppressive action of NS1 through interactions with numerous host proteins involved in the cellular innate immune response (3-5). Specifically, NS1 is well-known for its abrogation of the type I IFN response through interactions with pathogen recognition receptors and their activation partners such as the retinoic acid inducible gene I (RIG-I) and the E3-ubiquitin ligase TRIM25 (6-11).

RIG-I is an ATP-dependent cytoplasmic helicase whose primary function is to induce an antiviral signaling cascade in response to RNA virus infections (12,13). It contains two N-terminal caspase activation and recruitment domains (2CARDs), a central helicase domain consisting of 3 subdomains (Hel-1, Hel-2i, Hel-2), a linker domain (Br), and a regulatory C-terminal domain (CTD). RIG-I is predominantly activated by short 5'-triphosphorylated RNAs (5'ppp dsRNAs) such as those produced by the partial complementarity in the 5' and 3' UTRs of IAV genomic RNAs (13-16). As such, RIG-I is considered the main cytoplasmic sensor of IAV infection (17). Briefly, RIG-I undergoes a significant conformational change upon recognition of IAV RNAs that results in exposure and subsequent ubiquitination of the N-terminal 2CARDs by TRIM25 (18,19). Upon ubiquitination, RIG-I translocates to the mitochondria where it participates in a CARD/CARD interaction with the mitochondrial antiviral signaling protein (MAVS, also known as IPS-1, VISA, CARDIF) (20-22). This results in the recruitment of kinases IKK and TBK1 which function to phosphorylate the antiviral transcription factor IRF3 (23-25). Upon phosphorylation, IRF3 translocates to the nucleus and promotes transcription of type I IFNs, such as IFN- $\alpha/\beta$ .

Ubiquitination of the RIG-I 2CARDs by the E3-ubiquitin ligase TRIM25 is a critical step in the activation of the RIG-I signaling pathway (20,26,27). This step in the signaling pathway is inhibited during influenza infection by a direct interaction between NS1 and TRIM25 (6,26). While it has been shown that this interaction is a critical mechanism through which NS1 antagonizes RIG-I 2CARD ubiquitination (6,26),

it has not been shown whether additive antagonistic effects could result from additional direct interactions between NS1 and RIG-I. Recently, we reported that the NS1<sup>RBD</sup> from the 1918<sup>H1N1</sup> IAV (A/Brevig Mission/1/1918) interacts directly with the second CARD of RIG-I and that a naturally occurring mutation in the NS1<sup>RBD</sup> (R21Q) abrogated this direct interaction (8). Due to the critical role that the 2CARDs play in RIG-I activation, we hypothesized that this direct interaction would enhance the ability of NS1 to inhibit ubiquitination of the RIG-I 2CARDs. Furthermore, this inhibition would be independent of other previously studied NS1 interactions involving TRIM25 (6-11) and dsRNA structures (3) also known to inhibit the activation of RIG-I.

In this study, we demonstrate that the naturally occurring R21Q mutation in NS1 (NS1<sup>R21Q</sup>) significantly impacts NS1's ability to control RIG-I signaling. Specifically, we used reverse genetics to generate wild-type A/Puerto Rico/8/1934 IAV (rPR8<sup>WT</sup>) and a mutant IAV encoding the R21Q mutation in NS1 (rPR8<sup>R21Q</sup>) to test the effects of the mutation on aspects of the viral lifecycle. We observed that rPR8<sup>R21Q</sup> induced significantly more IRF3 phosphorylation and IFN- $\beta$  expression when compared to rPR8<sup>WT</sup>. These data indicate that rPR8<sup>R21Q</sup> is a significantly more potent RIG-I activator when compared to rPR8<sup>WT</sup>. Further analysis revealed that NS1<sup>R21Q</sup> is significantly less efficient at inhibiting TRIM25-dependent ubiquitination of the RIG-I 2CARDs, a critical step in the activation of RIG-I signaling. Additionally, we determined that the R21Q mutation markedly diminished the ability of NS1 to interact with the RIG-I 2CARDs. Finally, we confirmed that the R21Q mutation did not have an effect on any of the other NS1 functions known to inhibit the RIG-I pathway. Taken together, this is the first study to identify a natural polymorphism in the NS1<sup>RBD</sup> that mitigates its ability to control RIG-I 2CARD ubiquitination by TRIM25. These studies demonstrate that not only do strain-specific polymorphisms in NS1 have a significant impact on its ability to efficiently antagonize RIG-I activation, but the effects of these polymorphisms may be conditional to species-specific activation of RIG-I.

## RESULTS

Previously, we demonstrated that an R21Q mutation in the NS1<sup>RBD</sup> abrogated its ability to interact with the second CARD domain of RIG-I. Residue 21 is distal to other residues in the NS1<sup>RBD</sup> (R35, R38, K41) that are known to have functions in RNA binding and NS1 cellular localization (Figure 1) (28-30). Disrupting these residues (R35, R38, K41) by mutation is well-known to cause significant defects in viral fitness including decreased replication and an inability to control the cellular antiviral response. What is not known, however, is the effect of the R21Q mutation on the viral lifecycle as mutations in this region of the NS1<sup>RBD</sup> have yet to be studied.

### ***The R21Q mutation has no effect on the overall structure of the NS1<sup>RBD</sup>***

Given that residue 21 is in an unstudied region of the NS1<sup>RBD</sup>, we first wanted to ensure there were no gross structural changes in the NS1<sup>RBD</sup> associated with the R21Q mutation. To assess any potential structural changes caused by the mutation, we used NMR to analyze the <sup>1</sup>H-<sup>15</sup>N heteronuclear single-quantum coherence (HSQC) spectra of both the wild-type NS1<sup>RBD</sup> (RBD<sup>WT</sup>) and the R21Q mutation (RBD<sup>R21Q</sup>). Both HSQC spectra show a single set of dispersed peaks indicative of a well-folded protein with a single, major conformation (Figure 2A). Because the NS1<sup>RBD</sup> is a symmetric homodimer, only 72 amide resonances were expected and ultimately observed (not including the side-chain amides of glutamine and asparagine) for both the RBD<sup>WT</sup> and RBD<sup>R21Q</sup>. We then obtained resonance assignments for RBD<sup>R21Q</sup> using three-dimensional NMR experiments such as the HNCACB and CBCA(CO)NH for further analysis. High quality triple-resonance spectra allowed backbone resonance assignments to be obtained for 70 of the 72 (97%) possible assigned residues of the RBD<sup>R21Q</sup>. Analysis of the <sup>13</sup>C<sub>α</sub> chemical shifts indicated that each monomer of the RBD<sup>R21Q</sup> mutant is composed of an α<sub>1</sub> – turn – α<sub>2</sub> – turn – α<sub>3</sub> (Figure 2B) (31). This six-helical dimeric structure of the RBD<sup>R21Q</sup> homodimer is consistent with both <sup>13</sup>C<sub>α</sub> chemical shift analysis of the RBD<sup>WT</sup> (Figure 2B) and our previously solved solution structure of the 1918<sup>H1N1</sup> NS1<sup>RBD</sup>.

### ***Characterization of rPR8<sup>WT</sup> and rPR8<sup>R21Q</sup> replication and NS1 cellular localization***

Because the NS1 R21Q mutation had not been previously characterized, it was critical to determine if the mutation impacted basic aspects of the viral lifecycle such as IAV replication and NS1 cellular localization. To accomplish this, we used a previously described IAV reverse genetics system (32) to generate and rescue recombinant A/Puerto Rico/8/1934 viruses encoding wild-type NS1 (rPR8<sup>WT</sup>) and R21Q NS1 mutant (rPR8<sup>R21Q</sup>). Upon infecting adenocarcinomic human alveolar basal epithelial (A549) cells at an MOI of 0.01, we observed no significant differences in viral replication between rPR8<sup>WT</sup> and rPR8<sup>R21Q</sup> (Figure 3A). Similarly, we observed no significant change in the cellular localization of NS1 in A549s infected with rPR8<sup>WT</sup> or rPR8<sup>R21Q</sup> at 12 hours post-infection (MOI 2) (Figure 3B). Given that R21Q is a naturally occurring mutation, it is unsurprising that replication and intracellular localization are not affected as numerous viruses capable of productive infection in humans also possess a Gln at position 21. However, the observation of similar replication kinetics does not adjudicate the question of whether the two viruses will result in differential activation of the RIG-I signaling pathway upon infection, nor is it prognostic of potential differences in virulence between the two viruses as influenza replication levels do not necessarily correlate with virulence (33,34).

### ***Infection with rPR8<sup>R21Q</sup> results in significantly increased IRF-3 phosphorylation and IFN-β expression when compared to rPR8<sup>WT</sup> infection***

Activation of the RIG-I pathway results in the phosphorylation of the antiviral transcription factor IRF3 which then translocates to the nucleus and induces transcription of type I interferons (e.g. IFN-β). IAV NS1 has been previously shown to inhibit IRF3-mediated signaling through its antagonism of the RIG-I pathway (9,35). Based on our previous data demonstrating that NS1<sup>R21Q</sup> is unable to interact with the second CARD of RIG-I, we hypothesized that rPR8<sup>R21Q</sup> would be less efficient at antagonizing RIG-I signaling. To test this hypothesis, we infected A549 cells with rPR8<sup>WT</sup> and rPR8<sup>R21Q</sup> (MOI = 2) to determine

respective levels of IRF3 phosphorylation at 6, 12, and 24 hours post-infection. We observed that infection with rPR8<sup>R21Q</sup> resulted in significantly increased IRF3 phosphorylation (Figure 4A and 4B) at 12 and 24 hours post-infection relative to rPR8<sup>WT</sup> levels. Furthermore, we note that these observed differences are not due to disparities in NS1 expression levels between the two viruses as NS1 expression was determined to be equal across all time points measured (Figure 4A; quantification not shown). These data suggest that a Gln at position 21 in NS1 results in significantly less efficient antagonism of the RIG-I signaling pathway without altering NS1 expression.

Given that phosphorylated IRF3 acts as a transcription factor for the upregulation of type I IFNs, a corresponding increase in IFN- $\beta$  expression upon infection with rPR8<sup>R21Q</sup> when compared to rPR8<sup>WT</sup> is expected. We observed significantly increased IFN- $\beta$  mRNA expression at all timepoints (Figure 4C) and significantly increased IFN- $\beta$  protein expression at 12- and 24-hours post-infection (Figure 4D) using the identical experimental conditions described previously. Increased IRF3 phosphorylation and IFN- $\beta$  mRNA and protein expression suggests that rPR8<sup>R21Q</sup> is a significantly more potent activator of the RIG-I pathway during infection.

### ***The R21Q mutation in NS1 results in increased IFN- $\beta$ promoter activation***

While increased IRF3 phosphorylation and IFN- $\beta$  induction during infection suggests that rPR8<sup>R21Q</sup> is less efficient at antagonizing RIG-I signaling, it does not provide specific information on the mechanistic underpinnings by which NS1 is antagonizing the RIG-I pathway. To overcome this limitation, we designed a series of experiments to probe how NS1<sup>WT</sup> and NS1<sup>R21Q</sup> affect specific steps of the RIG-I activation pathway. In addition to our hypothesis that NS1 directly inhibits ubiquitination of the RIG-I 2CARDs, NS1 has been previously been shown to suppress two additional steps in the RIG-I signaling pathway. These steps include NS1 potentially shielding dsRNA structures from cellular factors responsible for detecting viral infection (3) as well as inhibition of RIG-I ubiquitination through a direct interaction with

TRIM25 (6,26). Completion of these experiments would result in a more mechanistic understanding of the phenotypic differences observed between rPR8<sup>WT</sup> and rPR8<sup>R21Q</sup>.

We first sought to determine whether the difference in the ability of rPR8<sup>WT</sup> and rPR8<sup>R21Q</sup> to inhibit IRF3 phosphorylation and IFN- $\beta$  induction during viral infection could be recapitulated in a plasmid-based system. This was accomplished by transfecting HEK 293T cells with a reporter construct containing a minimal IFN- $\beta$  promoter driving firefly luciferase expression (p125-Luc), NS1<sup>WT</sup> or NS1<sup>R21Q</sup> expression constructs, and a renilla luciferase control vector. IFN- $\beta$  promoter activity was stimulated by infection with the Cantell strain of Sendai virus (SeV), a well-known RIG-I agonist (14,36), or co-transfection with a construct encoding GST-2CARDs. It is important to note that overexpression of the RIG-I 2CARDs alone induces IFN- $\beta$  promoter activity (27). In agreement with our viral results, and previously published reports, overexpression of NS1<sup>WT</sup> resulted in a marked decreased in IFN- $\beta$  promoter activity in cells stimulated with SeV (Figure 5A) and RIG-I GST-2CARDs (Figure 5B). When compared to NS1<sup>WT</sup>, overexpression of NS1<sup>R21Q</sup> led to significantly increased IFN- $\beta$  promoter activity under the same conditions. This suggests that the introduction of the R21Q mutation reduces the efficiency of this antagonism since all other amino acids that have been demonstrated to significantly affect this pathway (R38, K41, E96, E97) remain intact (6).

### ***The R21Q mutation decreases the ability of NS1 to inhibit ubiquitination of RIG-I 2CARDs by TRIM25***

Our previous study showing that the R21Q mutation abrogated the interaction between the NS1<sup>RBD</sup> and the second CARD domain of RIG-I led to our hypothesis that NS1<sup>R21Q</sup> would be less efficient at blocking ubiquitination of the RIG-I 2CARDs by TRIM25. To test this hypothesis, we used pulldown studies in which 293T cells were transfected with plasmids encoding GST-fused human RIG-I 2CARDs (GST-2CARDs), TRIM25, and either NS1<sup>WT</sup> or NS1<sup>R21Q</sup>. The GST-2CARDs fusion protein was pulled down using glutathione agarose beads and visualized by



western blot to assess the relative ubiquitination level of 2CARDS in the presence of either NS1<sup>WT</sup> or NS1<sup>R21Q</sup>. The use of the GST-2CARDS fusion protein as a method to determine the effect of viral proteins on RIG-I 2CARD ubiquitination has been described previously (6,20,26,37). Consistent with previous studies (6,26), there was a marked decrease in GST-2CARDS ubiquitination in the presence of NS1<sup>WT</sup> (Figure 6A). We also observed that NS1<sup>R21Q</sup> is less efficient at inhibiting the ubiquitination of 2CARDS by TRIM25 relative to NS1<sup>WT</sup>, thus confirming our hypothesis (Figure 6B). We note, however, that the ability to inhibit 2CARD ubiquitination was not completely abrogated as there was a significant decrease in ubiquitination of 2CARDS in the presence of NS1<sup>R21Q</sup> relative to the GFP control. From these data, it is clear that the R21Q polymorphism significantly decreases the ability of NS1 to inhibit ubiquitination of RIG-I 2CARDS.

The data presented thus far provides strong evidence that NS1<sup>R21Q</sup> is a less efficient RIG-I antagonist due to its inability to control RIG-I 2CARDS ubiquitination. However, it is important to confirm that the molecular basis of the observed differences is due to NS1<sup>R21Q</sup> being deficient in binding to the RIG-I 2CARDS. To accomplish this, 293T cells were transfected as above and GST-2CARD was pulled down. Probing for 3xFLAG-NS1<sup>WT</sup> and NS1<sup>R21Q</sup> in pulldown fractions revealed that indeed, NS1<sup>WT</sup> is capable of interacting with the RIG-I 2CARDS yet this interaction is markedly diminished for the NS1<sup>R21Q</sup> mutant (Figure 6C and 6D). In addition, the interaction between NS1<sup>WT</sup> and the RIG-I 2CARDS remains unchanged in the absence of TRIM25 (Figure 6C, lanes 6-7) indicating a direct interaction between NS1<sup>WT</sup> and the RIG-I 2CARDS. To ensure that the observed interaction between NS1 and 2CARDS was not due to non-specific interactions with GST or the GA-beads, we incorporated the necessary controls in the GST pulldown experiments (Figure 6E). These data agree with our previous study showing that NS1<sup>WT</sup> is capable of interacting directly with the second CARD of RIG-I and that the R21Q mutation disrupts the interaction. Furthermore, the inability of NS1<sup>R21Q</sup> to bind the RIG-I 2CARDS as efficiently as NS1<sup>WT</sup> provides a straightforward explanation for the observed

differences in ubiquitination of 2CARDS. Specifically, the direct interaction between NS1<sup>WT</sup> and RIG-I 2CARDS could physically obstruct ubiquitination of the second CARD of RIG-I either by TRIM25 or its ability to bind free floating ubiquitin chains. In contrast, NS1<sup>R21Q</sup> binding to RIG-I 2CARDS is largely abolished relative to NS1<sup>WT</sup>, resulting in significantly less suppression of RIG-I 2CARD ubiquitination.

### ***The R21Q mutation has no effect on the interaction between NS1 and TRIM25***

Although we demonstrated that the R21Q mutation in NS1 inhibits its ability to suppress ubiquitination of RIG-I 2CARDS, other potential mechanisms underlying the differences in IRF3 phosphorylation and IFN- $\beta$  induction observed during rPR8<sup>WT</sup> and rPR8<sup>R21Q</sup> infection remain. Consequently, it was necessary to determine the effect of the mutation on other known mechanisms by which NS1 interferes with RIG-I activation to obtain a more mechanistic insight. One example in which NS1 interferes with activation of the RIG-I pathway is through its direct interaction with TRIM25 (38). It was therefore necessary to determine if our initial observations were independent of this interaction or if this interaction was contributing to the mitigation of NS1 function observed for the R21Q mutation. To test this, 293T cells were transfected with HA-TRIM25 along with either a GFP control vector, 3xFLAG-NS1<sup>WT</sup>, or 3xFLAG-NS1<sup>R21Q</sup>. TRIM25 was immunoprecipitated using  $\alpha$ HA-agarose at 36 hours post transfection. Analysis of the immunoprecipitated fractions revealed that the R21Q mutation in NS1 has no effect on its ability to bind TRIM25 (Figure 7). This observation offers critical insight into the molecular underpinnings of our initial observation that the R21Q mutant NS1 is less efficient at suppressing RIG-I activation. These data combined with the data in Figure 4 suggest that the R21Q mutation in NS1 specifically affects NS1's ability to bind the RIG-I 2CARDS independent of its TRIM25 binding function. Furthermore, these data support our hypothesis that the enhanced RIG-I activation and induction of type I interferons are due to NS1<sup>R21Q</sup>'s deficiency in binding 2CARDS and not the interaction between NS1 and TRIM25.

### ***The R21Q mutation has no effect on the interaction between NS1 and RNA***

Another potential mechanism by which NS1 antagonizes the RIG-I pathway is through its binding of dsRNA structures. It has been posited that NS1 binds dsRNA structures to shield its presence in the cell from host proteins that have evolved to induce the antiviral signaling cascade in response to RNA virus infection (3). Assessing the R21Q mutation's effect on this interaction would allow us to interrogate another possible contributor to the differences we observed between during rPR8<sup>WT</sup> and rPR8<sup>R21Q</sup> infection. We employed fluorescence polarization anisotropy (FPA) to measure the binding affinity of a dsRNA structure to both the wild-type NS1<sup>RDB</sup> and the R21Q NS1<sup>RDB</sup> mutant. For this analysis, we chose to use a previously described dsRNA (39) to determine its binding affinity to the NS1<sup>RBD</sup> (Figure 8A). Analysis of the isotherms indicated that the R21Q mutation had no effect on the ability of NS1 to bind the dsRNA structure thus eliminating it as a potential contributor to our observed phenotype (Figure 8B). Specifically, the binding affinities ( $K_d$ ) to the dsRNA structure for NS1<sup>WT</sup> and NS1<sup>R21Q</sup> were measured to be  $27 \pm 0.95$  nM and  $28.6 \pm 1.2$  nM respectively. These data reinforce our hypothesis that the differences in IRF3 phosphorylation and IFN- $\beta$  induction observed during rPR8<sup>WT</sup> and rPR8<sup>R21Q</sup> infection are due to direct inhibition of ubiquitination of 2CARDs by NS1.

### ***In vivo characterization of the R21Q mutation in the mouse model***

Given our observations that the R21Q mutation decreases the ability of NS1 to inhibit ubiquitination of RIG-I 2CARDs by TRIM25, we sought to characterize the effect of the R21Q mutation *in vivo*. Two groups of 8 – 12 week old C57BL/6 mice were inoculated intranasally with 100 plaque forming units (pfu) of rPR8<sup>WT</sup> or rPR8<sup>R21Q</sup>. Each group of mice was monitored for 14 days post-infection for mortality (Figure 9A), weight loss (Figure 9B), changes in body temperature (Figure 9C), and signs of illness (Figure 9D). Following Institutional Animal Care and Use Committee (IACUC) guidelines, when body weight was reduced to 75% of the starting weight, mice were deemed moribund and were

euthanized. At the end of the study, 60% and 50% of the mice infected with the rPR8<sup>WT</sup> and rPR8<sup>R21Q</sup> viruses were euthanized by day 11 post-infection, respectively. In addition, both viruses caused nearly identical percentages and rates of weight loss that stopped on day 8. However, mice infected with rPR8<sup>R21Q</sup> regained this weight approximately 30% faster than mice infected with rPR8<sup>WT</sup>, weighing an average 99% of their starting weight days 12 post-infection. Mice infected with rPR8<sup>R21Q</sup> also experienced less severe clinical signs of illness when compared to those infected with rPR8<sup>WT</sup>. Taken together, the *in vivo* data suggests that that rPR8<sup>R21Q</sup> virus may be moderately less pathogenic when compared to rPR8<sup>WT</sup>, albeit at levels not determined to be statistically significant. We note that the mechanism of RIG-I activation is fundamentally different when comparing humans and mice (26). It is this species-specific difference in RIG-I activation that offers a potential explanation for the lack of significant effect *in vivo* despite our observation that rPR8<sup>R21Q</sup> results in significantly increased IRF3 phosphorylation, type I interferon induction, and TRIM25-dependent ubiquitination of RIG-I 2CARDs relative to rPR8<sup>WT</sup>. The potential species-specific nature of the R21Q mutation will be addressed in the discussion section of this manuscript.

### **DISCUSSION**

To date, several strain-specific polymorphisms in IAV NS1 have been described to have significant effects on NS1's function as an innate immune antagonist. However, the strain-specific polymorphisms that have been previously described are primarily involved with the ability of NS1 to bind RNA and its interaction with CPSF30 (30 kDa subunit of the cleavage and polyadenylation specificity factor) (28,40-42). While both of these interactions play a large part in the overall ability of NS1 to control the host cellular antiviral response, NS1 takes part in a large number of other interactions where the effect of strain-specific polymorphisms is not well-understood. In this study, we investigated whether a previously described (8) strain-specific polymorphism at residue 21 in the IAV NS1 has a measurable effect on its ability to inhibit RIG-I signaling (Figure 11). Using reverse genetics, we demonstrated that infection with rPR8<sup>R21Q</sup> results

in significantly increased IRF3 phosphorylation and type I interferon in comparison to rPR8<sup>WT</sup>. In agreement with these results, we observed that NS1<sup>R21Q</sup> results in significantly increased TRIM25-dependent ubiquitination of the RIG-I 2CARDS, a critical step in the activation of RIG-I. Furthermore, we observed that NS1<sup>WT</sup> is indeed capable of interacting with the RIG-I 2CARDS in a TRIM25-independent manner and that an R21Q mutation in the NS1<sup>RBD</sup> significantly interferes with this interaction. Finally, we determined that the R21Q mutation had no observable effect on the ability of NS1 to bind dsRNA structures nor TRIM25. Collectively, these data indicate that NS1<sup>R21Q</sup> is less efficient at blocking ubiquitination of RIG-I 2CARDSs leading to a more potent activation of the RIG-I signaling pathway. A schematic of RIG-I activation in the context of influenza infection with specific steps at which NS1 suppresses activation of RIG-I is illustrated in Figure 11.

A critical step in the activation of the RIG-I signaling pathway is ubiquitination of RIG-I 2CARDS by TRIM25. This predominantly occurs by TRIM25 covalently attaching ubiquitin chains to K172 in the second CARD of RIG-I via a direct interaction between the SPRY domain of TRIM25 and the 2CARDS of RIG-I (20). Alternatively, free-floating ubiquitin chains synthesized by TRIM25 can bind directly to RIG-I 2CARDS. (43). Given that the R21Q mutation in NS1 has no effect on TRIM25, the differences observed in NS1<sup>WT</sup> and NS1<sup>R21Q</sup> function should be independent of the ability of NS1 to abrogate TRIM25 function. Therefore, these data can be explained by two distinct mechanisms in which a strain-specific, direct interaction between NS1 and RIG-I 2CARDS enhances NS1's ability to mitigate K172 ubiquitination. The first is that NS1 proteins capable of binding to the RIG-I 2CARDS obstruct access of TRIM25 to the CARDS, resulting in blockage of ubiquitination. Alternatively, the NS1:2CARD interaction interferes with the 2CARDS ability to bind free floating ubiquitin chains. It should be noted that these possibilities are not necessarily mutually exclusive. For example, it is possible that NS1 proteins capable of binding the RIG-I 2CARDS could interfere with both of these mechanisms. In either scenario, NS1 proteins encoding a Gln at

position 21 would rely solely on their ability to inhibit TRIM25, resulting in significantly less efficient suppression of RIG-I 2CARD ubiquitination. Future studies aimed at fully characterizing the structural interplay between NS1 and the RIG-I 2CARDS will reveal the mechanism by which this direct interaction interferes with activation of the RIG-I signaling pathway.

While this study and our previous work provide information on the molecular basis for how polymorphisms at residue 21 affects NS1s interaction with the RIG-I 2CARDS, they do not address a particularly outstanding question: Why does this polymorphism occur when it results in an increased antiviral response during infection? Collective analysis of all available NS1 sequences indicated that arginine is the predominant amino acid at position 21 (Figure 10A). However, this predominance was not maintained when sequences were analyzed as a function of host species or serotype (Figure 10B). NS1 proteins derived from serotypes that usually result in seasonal epidemics (H1N1/H3N2) have a clear disparity in the identity of residue 21. NS1 proteins derived from H1N1 serotypes predominantly have an Arg while those derived from H3N2 strains predominantly have a Gln at position 21. Additionally, residue 21 identity in IAV subtypes generally regarded as highly pathogenic (H5N1/H7N9) are heavily biased toward Arg. It is plausible that these differences are the result of species-specific adaptation as it has already been determined that NS1s interference with RIG-I ubiquitination differs significantly between humans and mice (26). It is this difference in RIG-I activation that offers a potential explanation for our *in vivo* data. Specifically, it has been previously reported that NS1 does not antagonize the RIG-I signaling cascade in mice by preventing 2CARDS ubiquitination during IAV infection (44,45). Instead, NS1 prevents ubiquitination of RIG-I in regions of the protein distal to the 2CARDS which ultimately lead to RIG-I activation in mice (26). This is due to the fact that activation of human RIG-I requires Lys63-linked ubiquitination of Lys172 by TRIM25 ubiquitin E3 ligase (20) while murine RIG-I lacks Lys172 in 2CARDS (26). Because the R21Q mutation specifically

abrogates the NS1<sup>RBD</sup>'s interaction with 2CARD of RIG-I (8), it is likely that the species-specific differences in RIG-I activation underlie the marginal differences observed in the murine infection model used in this study.

Going forward we believe it will be important to address this question by assessing how efficiently NS1 proteins from multiple strains of IAV isolated from multiple species are able to antagonize RIG-I 2CARDs ubiquitination. Of particular interest for future studies will be to determine how differential antagonism of RIG-I 2CARDs ubiquitination contributes to virulence during IAV infection. Taken together, the work presented in this study demonstrate that NS1 is capable of additional sequence-specific interactions with RIG-I to facilitate its antagonism of the cellular antiviral response. It stresses the importance of how strain-specific polymorphisms in NS1 can affect its ability to antagonize the host cellular immune response in ways that are yet to be appreciated. This knowledge provides a solid foundation for further investigation into the structural and molecular mechanisms that define how these strain-specific polymorphisms in NS1 affect its ability to inhibit the RIG-I pathway. Understanding strain-specific differences in coping with the host antiviral response may better prepare us to predict the pandemic potential of IAV and aid in the development of vaccines and antivirals.

## EXPERIMENTAL PROCEDURES

### *Plasmids and Cloning*

The pEBG-GST and pGST-2CARD plasmids were kind gifts from Dr. Michaela Gack and their construction and purpose was described previously (20,26,27). The HA-TRIM25 construct was generated by RT-PCR from total RNA isolated from primary normal human bronchiolar epithelial cells (nHBE) with the following primers, Forward 5' GAT CAT GCT AGC ATG GCA GAG CTG TGC CCC CTG 3' and Reverse 5' GAT CAT GAA TTC CTA CTT GGG GGA GCA GAT GGA 3'. TRIM25 was inserted into an existing vector (Addgene 18712) using the NheI and EcoRI restriction sites. Giving TRIM25 an N-terminal HA tag. The p125-Luc construct was a kind gift from Dr. Takashi Fujita and its construction was described previously.

The pCMV-rLuc was a kind gift from Dr. Mengxi Xiang (UAB). Construction of the influenza reverse genetics plasmids for the A/Puerto Rico/8/1934 strain was described previously (32). The R21Q mutant NS segment was generated using inverse mutagenesis PCR with the following primers: Forward 5' Phos – CTT TGG CAT GTC CGC AAA CAG GTT GCA GAC CAA GAA CTA 3' and Reverse 5' Phos – AAA GCA ATC TAC CTG AAA GCT TGA CAC AGT GTT TGG ATC 3'. 3xFLAG-NS1<sup>WT</sup> and 3xFLAG-NS1<sup>R21Q</sup> expression constructs were generated by amplifying NS1 from the IAV reverse genetics plasmids used to rescue the viruses to ensure continuity between overexpression and infection studies. NS1<sup>WT</sup> and NS1<sup>R21Q</sup> were cloned into the p3xFLAG vector (Sigma) between the EcoRI and SmaI restriction sites using the following primers: Forward 5' GAT CAT GAA TTC AAT GGA TCC AAA CAC TGT GTC AAG CTT T 3' and Reverse 5' GAT CAT CCC GGG GTC AAA CTT CTG ACC TAA TTG TTC CCG CCA T 3'.

### *NMR Spectroscopy*

NMR experiments were carried out at 25°C using Bruker Avance III spectrometers equipped with TCI cryoprobes operating at 600 Mhz and 850 Mhz <sup>1</sup>H frequencies. All NMR data were processed using NMRPipe (46) and analyzed using NMRView (47) compiled on Linux workstations. Backbone <sup>1</sup>H, <sup>13</sup>C, and <sup>15</sup>N resonances were assigned using standard triple-resonance assignment experiments: HNCACB & CBCA(CO)NH (48).

### *Viruses and Infections*

Recombinant A/Puerto Rico/8/1934 (rPR8) viruses were rescued as described previously (32). Stocks of rPR8<sup>WT</sup> and rPR8<sup>R21Q</sup> were generated by low MOI propagation on Madine-Darby canine kidney cells (MDCK) in 1x serum-free EMEM (SF EMEM) supplemented with 3µg/mL TPCK treated trypsin (Worthington Biochemical). Stock IAV viruses were titered using traditional plaque assays on MDCKs. All recombinant viruses were sequence verified by Sanger sequencing. A549 type 2 alveolar epithelial cells were infected with rPR8<sup>WT</sup> and/or rPR8<sup>R21Q</sup> at the given MOI for 1hr in SF EMEM. After the 1hr adsorption, the inoculum was



removed and replaced with fresh SF EMEM. Sendai virus (Cantell strain, ATCC VR-907) was propagated in ten-day old SPF chicken embryos in accordance with established IACUC protocols. Stock Sendai virus was titrated using hemmagglutination assays.

### ***Pulldowns and Immunoprecipitations***

For GST pulldown experiments, 293T cells were transfected with a control vector pEBG-GST or pGST-2CARDs along with pHA-TRIM25 and either 3xFLAG-NS1<sup>WT</sup> or 3xFLAG-NS1<sup>R21Q</sup>. 36 hours post transfection cells were lysed in GST lysis buffer (50mM Tris, 200mM NaCl, 1% Triton X-100, pH 7.5) and an equal amount of protein was added to glutathione agarose (GA) beads (Pierce;16100). Lysates were incubated with the GA beads for 2 hours at room temperature in a tube rotator. After incubation, the beads were collected at 1000 xG for 2 minutes and washed with GST wash buffer (50mM Tris, 200mM NaCl, pH 7.5). Washing was repeated 3 times. Bound protein was eluted in 1X Laemmli buffer with beta-mercaptoethanol by heating at 95C for 5 minutes. Samples were then assayed by immunoblot.

For HA specific immunoprecipitations, 293T cells were transfected with pHA-TRIM25 and either a GFP control vector, p3xFLAG-NS1<sup>WT</sup>, or p3xFLAG-NS1<sup>R21Q</sup>. 36 hours post-infection, cells were lysed in TBS lysis buffer (50mM Tris, 200mM NaCl, 1% Triton X-100, pH 7.5) and an equal amount of protein was added to anti-HA agarose beads (Pierce; 26181). Lysates were incubated with anti-HA beads for 6 hours at 4C. After incubation, the beads were collected at 12,000 xG for 3 seconds and washed with TBS wash buffer (50mM Tris, 200mM NaCl, 0.05% Tween-20, pH 7.5). Washing steps were repeated three times. Beads were resuspended in 2x Laemmli buffer without  $\beta$ -mercaptoethanol and heated at 95C for 5 minutes. Samples were then assayed by immunoblot.

### ***IFN- $\beta$ promoter activity assays***

293T cells were transfected with p125-Luc and either a GFP expression vector or 3xFLAG-NS1<sup>WT</sup> or 3xFLAG-NS1<sup>R21Q</sup> along with pCMV-rLuc as a control for transfection efficiency. 36 hours post transfection, cells were infected with

200 HAU of Sendai virus for 16-18 hours. After infection, luminescence was measured using a dual-luciferase assay (Promega) on a Cytation 5 microplate reader (Biotek).

### ***Confocal Microscopy***

A549 cells were grown on coverslips and infected at 80% confluence with rPR8<sup>WT</sup> or rPR8<sup>R21Q</sup> at an MOI of 5. At 12 hours post infection (hpi), the coverslips were fixed with 4% paraformaldehyde (PFA) for 15 minutes at 25°C. The fixed cells were then blocked and permeabilized in phosphate buffered saline (PBS) containing 5% Goat Serum and 0.5% Triton X-100 for 1 hour @ 25°C. Cells were then stained with an anti-NS1 primary antibody (Kerafast EMB005) at a 1:200 dilution in PBS containing 5% Goat Serum and 0.3% Triton X-100 for 2 hours at 25°C and subsequently washed 5x with PBS + 0.1% Tween-20 (PBST). Cells were then stained with an Alexa Fluor 488 conjugated goat anti-mouse IgG<sub>2B</sub> secondary antibody (Life Technologies A21141) for 30 minutes at 25°C followed by 5 PBST washes. Cells were then treated with DAPI (1:1000 in PBST) for 10 minutes @ 25°C and washed 3x with PBST. Finally, coverslips were mounted onto microscope slides using Permafluor Aqueous Mounting Medium (Thermo Scientific) and sealed using nail polish. Images were acquired using an Olympus FV1000 confocal microscope and Olympus Fluoview FV10 ASW 4.2 software. All images were acquired using at 100X magnification with an additional 1.3X digital zoom.

### ***Western Blots and ELISA***

Whole cell lysates (GST lysis buffer or M-PER; Pierce 78501) were separated by SDS-PAGE (Bio-Rad Criterion TGX) and transferred to nitrocellulose membrane according to manufacturer's protocols (Bio-Rad). After blocking in 5% non-fat dry milk in TBST (10mM Tris, 150mM NaCl, 0.5% Tween-20, pH 8) for one hour, the membrane was washed once with TBST and incubated with antibodies against GST (CST; 2624), FLAG (Sigma; X), B-Actin (SCBT, 47778), IAV NS1 (SCBT; 130568), total IRF3 (CST;11904), phosphor-IRF3 (CST;4947), and RIG-I (CST;3743) in TBST at 4C overnight. Membranes were washed three times in TBST for

15 minutes and membranes were incubated with HRP-conjugated anti-mouse or anti-rabbit secondary antibodies for 1 hour at room-temperature in 5% NFDM. Blots were washed as before and developed with Clarity ECL (Bio-Rad). Blots were imaged on a Chemi-Doc imager. ELISA for IFN- $\beta$  in cell culture supernatants was done following manufacturer's instructions (PBL Assay Science). Densitometry of western blots was analyzed using Bio-Rad Image Lab.

### **Quantitative PCR**

A549 cells were lysed with buffer RLT (Qiagen) and total RNA was extracted using the Qiagen RNeasy Plus kit with gDNA eliminator columns. 60 ng of total RNA was used per reaction. Real-time analysis for IFN- $\beta$  and  $\beta$ -actin was performed iTaq one-step SYBR qPCR kit (Bio-Rad) following the manufacturer's instructions. Relative IFN- $\beta$  mRNA values were normalized according to B-actin expression levels. The fold change of mRNA expression was calculated using the  $\Delta\Delta CT$  method (Bio-Rad CFX Manager). The specificity of each amplicon was determined by analyzing its corresponding melting curve. The sequences of primers used in qPCR reactions are as follows: IFN- $\beta$ : Forward 5' TGG GAG GCT TGA ATA CTG CCT CAA 3' and Reverse 5' TCT CAT AGA TGG TCA ATG CGG CGT 3'.  $\beta$ -Actin: Forward 5' ACC AAC TGG GAC GAC ATG GAG AAA 3' and Reverse 5' TAG CAC AGC CTG GAT AGC AAC GTA 3'.

### **Fluorescence Polarization**

Fluorescence polarization (FP) experiments were carried out using purified WT and R21Q mutant 1918<sup>H1N1</sup> NS1<sup>RBD</sup>s and 5' 6-FAM labeled short hairpin RNA (shDM03) (39). Purification of the NS1<sup>RBD</sup>s was carried out as described previously (8). 5' 6-FAM labeled shDM03 was commercially synthesized (IDT). Prior to binding experiments, NS1<sup>RBD</sup>s and 5' 6-FAM shDM03 were dialyzed against FP buffer (50mM Tris-HCL, 100 mM NaCl, 1mM EDTA, pH 8) to ensure buffer matching across samples. FP experiments were conducted with a constant concentration of shDM03 (5 nM) in the presence of increasing concentrations of the NS1<sup>RBD</sup>s. Once mixed, samples were incubated at room

temperature for 1 hour and then FP measurements were made on a Victor X5 microplate reader (Perkin Elmer) using the FP-Flourescein protocol with excitation and emission at 485 and 535 nm respectively and a counting time of 1 second. Change in polarization was determined by subtracting FP measurements of shDM03 buffer only controls from experimental samples.

### **C57BL/6 Infections**

Male and Female 8-12 week old C57BL/6 mice were obtained from Taconic Biosciences (Rensselaer, New York). Mice were intranasally inoculated with 100 pfu of either A/PR8/1934-NS1<sup>WT</sup> or A/PR8/1934-NS1<sup>R21Q</sup>. Mice were monitored daily for 14 days post-infection for changes in weight, temperature, and clinical signs. Percent changes in clinical criteria were determined by comparison to pre-infection values for each mouse. Mice were euthanized by intraperitoneal injection of Euthasol (200mg kg<sup>-1</sup>) when deemed moribund according to Institutional Animal Care and Use Committee (IACUC) guidelines.

### **ACKNOWLEDGEMENTS**

We thank Dr. Michaela Gack for kindly providing us with the pGST-2CARD and pEBG-GST empty vector, Dr. Adolfo Garcia-Sastre for providing us with the PR8 reverse genetics constructs, and Dr. Takashi Fujita for kindly providing us with the p125-Luc vector. We would also like to thank the Placzek lab for their technical assistance in collecting the FPA data. This work was funded by NIH grants AI134693 (C.M.P.) and AI111475 (K.S.H). A.S.J. was supported by the NIH Training Program in Cell, Molecular, and Developmental Biology grant T32GM008111-31. The Bruker 850 MHz and 600 MHz magnets used herein were funded by NCI Grant 1P30 CA-13148, NCI Grant 1S10 RR022994-01A1, and NCI Grant 1P30 CA-13148.

### **CONFLICT OF INTEREST**

No author has an actual or perceived conflict of interest with the contents of this article. The content is solely the responsibility of the authors and does not necessarily represent the official views of the National Institutes of Health.

## REFERENCES

1. Thompson, W. W., Comanor, L., and Shay, D. K. (2006) Epidemiology of seasonal influenza: use of surveillance data and statistical models to estimate the burden of disease. *J Infect Dis* **194 Suppl 2**, S82-91
2. Molinari, N. A., Ortega-Sanchez, I. R., Messonnier, M. L., Thompson, W. W., Wortley, P. M., Weintraub, E., and Bridges, C. B. (2007) The annual impact of seasonal influenza in the US: measuring disease burden and costs. *Vaccine* **25**, 5086-5096
3. Ayllon, J., and Garcia-Sastre, A. (2015) The NS1 protein: a multitasking virulence factor. *Curr Top Microbiol Immunol* **386**, 73-107
4. Hale, B. G., Randall, R. E., Ortin, J., and Jackson, D. (2008) The multifunctional NS1 protein of influenza A viruses. *J Gen Virol* **89**, 2359-2376
5. Krug, R. M. (2015) Functions of the influenza A virus NS1 protein in antiviral defense. *Curr Opin Virol* **12**, 1-6
6. Gack, M. U., Albrecht, R. A., Urano, T., Inn, K. S., Huang, I. C., Carnero, E., Farzan, M., Inoue, S., Jung, J. U., and Garcia-Sastre, A. (2009) Influenza A virus NS1 targets the ubiquitin ligase TRIM25 to evade recognition by the host viral RNA sensor RIG-I. *Cell Host Microbe* **5**, 439-449
7. Guo, Z., Chen, L. M., Zeng, H., Gomez, J. A., Plowden, J., Fujita, T., Katz, J. M., Donis, R. O., and Sambhara, S. (2007) NS1 protein of influenza A virus inhibits the function of intracytoplasmic pathogen sensor, RIG-I. *Am J Respir Cell Mol Biol* **36**, 263-269
8. Jureka, A. S., Kleinpeter, A. B., Cornilescu, G., Cornilescu, C. C., and Petit, C. M. (2015) Structural Basis for a Novel Interaction between the NS1 Protein Derived from the 1918 Influenza Virus and RIG-I. *Structure* **23**, 2001-2010
9. Mibayashi, M., Martinez-Sobrido, L., Loo, Y. M., Cardenas, W. B., Gale, M., Jr., and Garcia-Sastre, A. (2007) Inhibition of retinoic acid-inducible gene I-mediated induction of beta interferon by the NS1 protein of influenza A virus. *J Virol* **81**, 514-524
10. Opitz, B., Rejaibi, A., Dauber, B., Eckhard, J., Vinzing, M., Schmeck, B., Hippenstiel, S., Suttorp, N., and Wolff, T. (2007) IFNbeta induction by influenza A virus is mediated by RIG-I which is regulated by the viral NS1 protein. *Cell Microbiol* **9**, 930-938
11. Pichlmair, A., Schulz, O., Tan, C. P., Naslund, T. I., Liljestrom, P., Weber, F., and Reis e Sousa, C. (2006) RIG-I-mediated antiviral responses to single-stranded RNA bearing 5'-phosphates. *Science* **314**, 997-1001
12. Yoneyama, M., Kikuchi, M., Natsukawa, T., Shinobu, N., Imaizumi, T., Miyagishi, M., Taira, K., Akira, S., and Fujita, T. (2004) The RNA helicase RIG-I has an essential function in double-stranded RNA-induced innate antiviral responses. *Nat Immunol* **5**, 730-737
13. Yoneyama, M., Onomoto, K., Jogi, M., Akaboshi, T., and Fujita, T. (2015) Viral RNA detection by RIG-I-like receptors. *Curr Opin Immunol* **32**, 48-53
14. Rehwinkel, J., Tan, C. P., Goubau, D., Schulz, O., Pichlmair, A., Bier, K., Robb, N., Vreede, F., Barclay, W., Fodor, E., and Reis e Sousa, C. (2010) RIG-I detects viral genomic RNA during negative-strand RNA virus infection. *Cell* **140**, 397-408
15. Schlee, M., Roth, A., Hornung, V., Hagmann, C. A., Wimmenauer, V., Barchet, W., Coch, C., Janke, M., Mihailovic, A., Wardle, G., Juraneck, S., Kato, H., Kawai, T., Poeck, H., Fitzgerald, K. A., Takeuchi, O., Akira, S., Tuschl, T., Latz, E., Ludwig, J., and Hartmann, G.

- (2009) Recognition of 5' triphosphate by RIG-I helicase requires short blunt double-stranded RNA as contained in panhandle of negative-strand virus. *Immunity* **31**, 25-34
16. Hornung, V., Ellegast, J., Kim, S., Brzozka, K., Jung, A., Kato, H., Poeck, H., Akira, S., Conzelmann, K. K., Schlee, M., Endres, S., and Hartmann, G. (2006) 5'-Triphosphate RNA is the ligand for RIG-I. *Science* **314**, 994-997
  17. Baum, A., Sachidanandam, R., and Garcia-Sastre, A. (2010) Preference of RIG-I for short viral RNA molecules in infected cells revealed by next-generation sequencing. *Proc Natl Acad Sci U S A* **107**, 16303-16308
  18. Ramanathan, A., Devarkar, S. C., Jiang, F., Miller, M. T., Khan, A. G., Marcotrigiano, J., and Patel, S. S. (2016) The autoinhibitory CARD2-Hel2i Interface of RIG-I governs RNA selection. *Nucleic Acids Res* **44**, 896-909
  19. Kolakofsky, D., Kowalinski, E., and Cusack, S. (2012) A structure-based model of RIG-I activation. *RNA* **18**, 2118-2127
  20. Gack, M. U., Shin, Y. C., Joo, C. H., Urano, T., Liang, C., Sun, L., Takeuchi, O., Akira, S., Chen, Z., Inoue, S., and Jung, J. U. (2007) TRIM25 RING-finger E3 ubiquitin ligase is essential for RIG-I-mediated antiviral activity. *Nature* **446**, 916-920
  21. Jiang, X., Kinch, L. N., Brautigam, C. A., Chen, X., Du, F., Grishin, N. V., and Chen, Z. J. (2012) Ubiquitin-induced oligomerization of the RNA sensors RIG-I and MDA5 activates antiviral innate immune response. *Immunity* **36**, 959-973
  22. Hou, F., Sun, L., Zheng, H., Skaug, B., Jiang, Q. X., and Chen, Z. J. (2011) MAVS forms functional prion-like aggregates to activate and propagate antiviral innate immune response. *Cell* **146**, 448-461
  23. Kawai, T., Takahashi, K., Sato, S., Coban, C., Kumar, H., Kato, H., Ishii, K. J., Takeuchi, O., and Akira, S. (2005) IPS-1, an adaptor triggering RIG-I- and Mda5-mediated type I interferon induction. *Nat Immunol* **6**, 981-988
  24. Seth, R. B., Sun, L., Ea, C. K., and Chen, Z. J. (2005) Identification and characterization of MAVS, a mitochondrial antiviral signaling protein that activates NF-kappaB and IRF 3. *Cell* **122**, 669-682
  25. Xu, L. G., Wang, Y. Y., Han, K. J., Li, L. Y., Zhai, Z., and Shu, H. B. (2005) VISA is an adapter protein required for virus-triggered IFN-beta signaling. *Mol Cell* **19**, 727-740
  26. Rajsbaum, R., Albrecht, R. A., Wang, M. K., Maharaj, N. P., Versteeg, G. A., Nistal-Villan, E., Garcia-Sastre, A., and Gack, M. U. (2012) Species-specific inhibition of RIG-I ubiquitination and IFN induction by the influenza A virus NS1 protein. *PLoS Pathog* **8**, e1003059
  27. Gack, M. U., Kirchhofer, A., Shin, Y. C., Inn, K. S., Liang, C., Cui, S., Myong, S., Ha, T., Hopfner, K. P., and Jung, J. U. (2008) Roles of RIG-I N-terminal tandem CARD and splice variant in TRIM25-mediated antiviral signal transduction. *Proc Natl Acad Sci U S A* **105**, 16743-16748
  28. Cheng, A., Wong, S. M., and Yuan, Y. A. (2009) Structural basis for dsRNA recognition by NS1 protein of influenza A virus. *Cell Res* **19**, 187-195
  29. Melen, K., Kinnunen, L., Fagerlund, R., Ikonen, N., Twu, K. Y., Krug, R. M., and Julkunen, I. (2007) Nuclear and nucleolar targeting of influenza A virus NS1 protein: striking differences between different virus subtypes. *J Virol* **81**, 5995-6006



30. Greenspan, D., Palese, P., and Krystal, M. (1988) Two nuclear location signals in the influenza virus NS1 nonstructural protein. *J Virol* **62**, 3020-3026
31. Wishart, D. S., and Sykes, B. D. (1994) The <sup>13</sup>C chemical-shift index: a simple method for the identification of protein secondary structure using <sup>13</sup>C chemical-shift data. *Journal of biomolecular NMR* **4**, 171-180
32. Quinlivan, M., Zamarin, D., Garcia-Sastre, A., Cullinane, A., Chambers, T., and Palese, P. (2005) Attenuation of equine influenza viruses through truncations of the NS1 protein. *J Virol* **79**, 8431-8439
33. Askovich, P. S., Sanders, C. J., Rosenberger, C. M., Diercks, A. H., Dash, P., Navarro, G., Vogel, P., Doherty, P. C., Thomas, P. G., and Aderem, A. (2013) Differential host response, rather than early viral replication efficiency, correlates with pathogenicity caused by influenza viruses. *PLoS One* **8**, e74863
34. Fan, S., Hatta, M., Kim, J. H., Halfmann, P., Imai, M., Macken, C. A., Le, M. Q., Nguyen, T., Neumann, G., and Kawaoka, Y. (2014) Novel residues in avian influenza virus PB2 protein affect virulence in mammalian hosts. *Nat Commun* **5**, 5021
35. Talon, J., Horvath, C. M., Polley, R., Basler, C. F., Muster, T., Palese, P., and Garcia-Sastre, A. (2000) Activation of interferon regulatory factor 3 is inhibited by the influenza A virus NS1 protein. *J Virol* **74**, 7989-7996
36. Baum, A., and Garcia-Sastre, A. (2011) Differential recognition of viral RNA by RIG-I. *Virulence* **2**, 166-169
37. Sanchez-Aparicio, M. T., Feinman, L. J., Garcia-Sastre, A., and Shaw, M. L. (2018) Paramyxovirus V Proteins Interact with the RIG-I/TRIM25 Regulatory Complex and Inhibit RIG-I Signaling. *J Virol* **92**
38. Koliopoulos, M. G., Lethier, M., van der Veen, A. G., Haubrich, K., Hennig, J., Kowalinski, E., Stevens, R. V., Martin, S. R., Reis, E. S. C., Cusack, S., and Rittinger, K. (2018) Molecular mechanism of influenza A NS1-mediated TRIM25 recognition and inhibition. *Nat Commun* **9**, 1820
39. Marc, D., Barbachou, S., and Soubieux, D. (2013) The RNA-binding domain of influenzavirus non-structural protein-1 cooperatively binds to virus-specific RNA sequences in a structure-dependent manner. *Nucleic Acids Res* **41**, 434-449
40. Cheng, J., Zhang, C., Tao, J., Li, B., Shi, Y., and Liu, H. (2018) Effects of the S42 residue of the H1N1 swine influenza virus NS1 protein on interferon responses and virus replication. *Virol J* **15**, 57
41. Dankar, S. K., Miranda, E., Forbes, N. E., Pelchat, M., Tavassoli, A., Selman, M., Ping, J., Jia, J., and Brown, E. G. (2013) Influenza A/Hong Kong/156/1997(H5N1) virus NS1 gene mutations F103L and M106I both increase IFN antagonism, virulence and cytoplasmic localization but differ in binding to RIG-I and CPSF30. *Virol J* **10**, 243
42. Dankar, S. K., Wang, S., Ping, J., Forbes, N. E., Keleta, L., Li, Y., and Brown, E. G. (2011) Influenza A virus NS1 gene mutations F103L and M106I increase replication and virulence. *Virol J* **8**, 13
43. Zeng, W., Sun, L., Jiang, X., Chen, X., Hou, F., Adhikari, A., Xu, M., and Chen, Z. J. (2010) Reconstitution of the RIG-I pathway reveals a signaling role of unanchored polyubiquitin chains in innate immunity. *Cell* **141**, 315-330

44. Oshiumi, H., Matsumoto, M., Hatakeyama, S., and Seya, T. (2009) Riplet/RNF135, a RING finger protein, ubiquitinates RIG-I to promote interferon-beta induction during the early phase of viral infection. *J Biol Chem* **284**, 807-817
45. Oshiumi, H., Miyashita, M., Inoue, N., Okabe, M., Matsumoto, M., and Seya, T. (2010) The ubiquitin ligase Riplet is essential for RIG-I-dependent innate immune responses to RNA virus infection. *Cell Host Microbe* **8**, 496-509
46. Delaglio, F., Grzesiek, S., Vuister, G. W., Zhu, G., Pfeifer, J., and Bax, A. (1995) Nmrpipe - a Multidimensional Spectral Processing System Based on Unix Pipes. *Journal of biomolecular NMR* **6**, 277-293
47. Johnson, B. A., and Blevins, R. A. (1994) NMR View: A computer program for the visualization and analysis of NMR data. *Journal of biomolecular NMR* **4**, 603-614
48. Muhandiram, D. R., and Kay, L. E. (1994) Gradient-Enhanced Triple-Resonance Three-Dimensional NMR Experiments with Improved Sensitivity. *Journal of Magnetic Resonance, Series B* **103**, 203-216
49. Peisley, A., Wu, B., Xu, H., Chen, Z. J., and Hur, S. (2014) Structural basis for ubiquitin-mediated antiviral signal activation by RIG-I. *Nature* **509**, 110-114

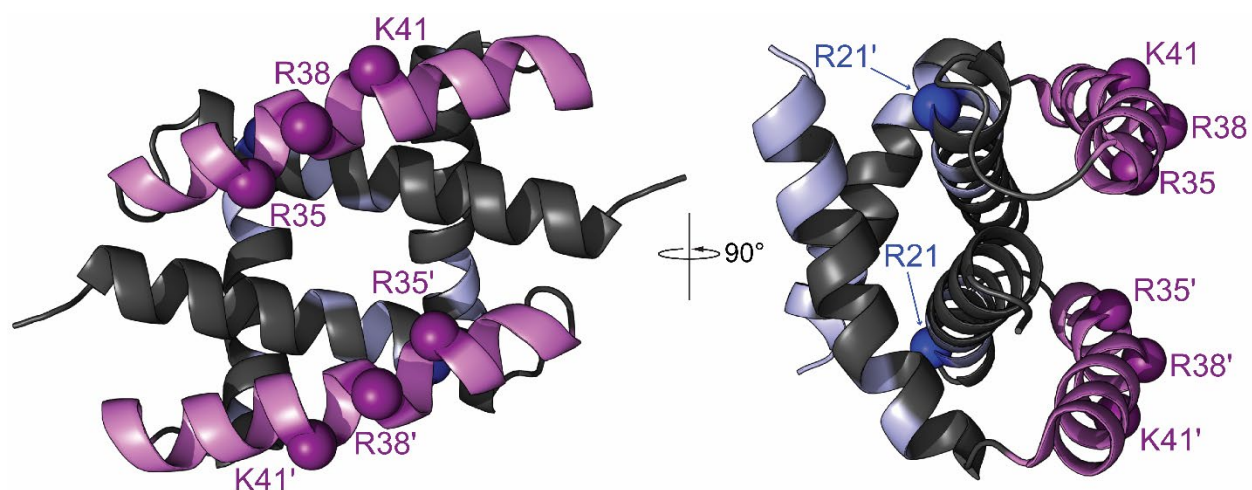


**Figure 1. Structure of the 1918<sup>H1N1</sup> NS1<sup>RBD</sup>.** The RNA binding interface is indicated in light purple while the interface determined to interact with the second CARD of RIG-I is indicated in light blue. Residues known to play critical roles in RNA binding and localization (R35, R38, K41) and the focus of our studies (R21) are depicted by spheres and labeled.

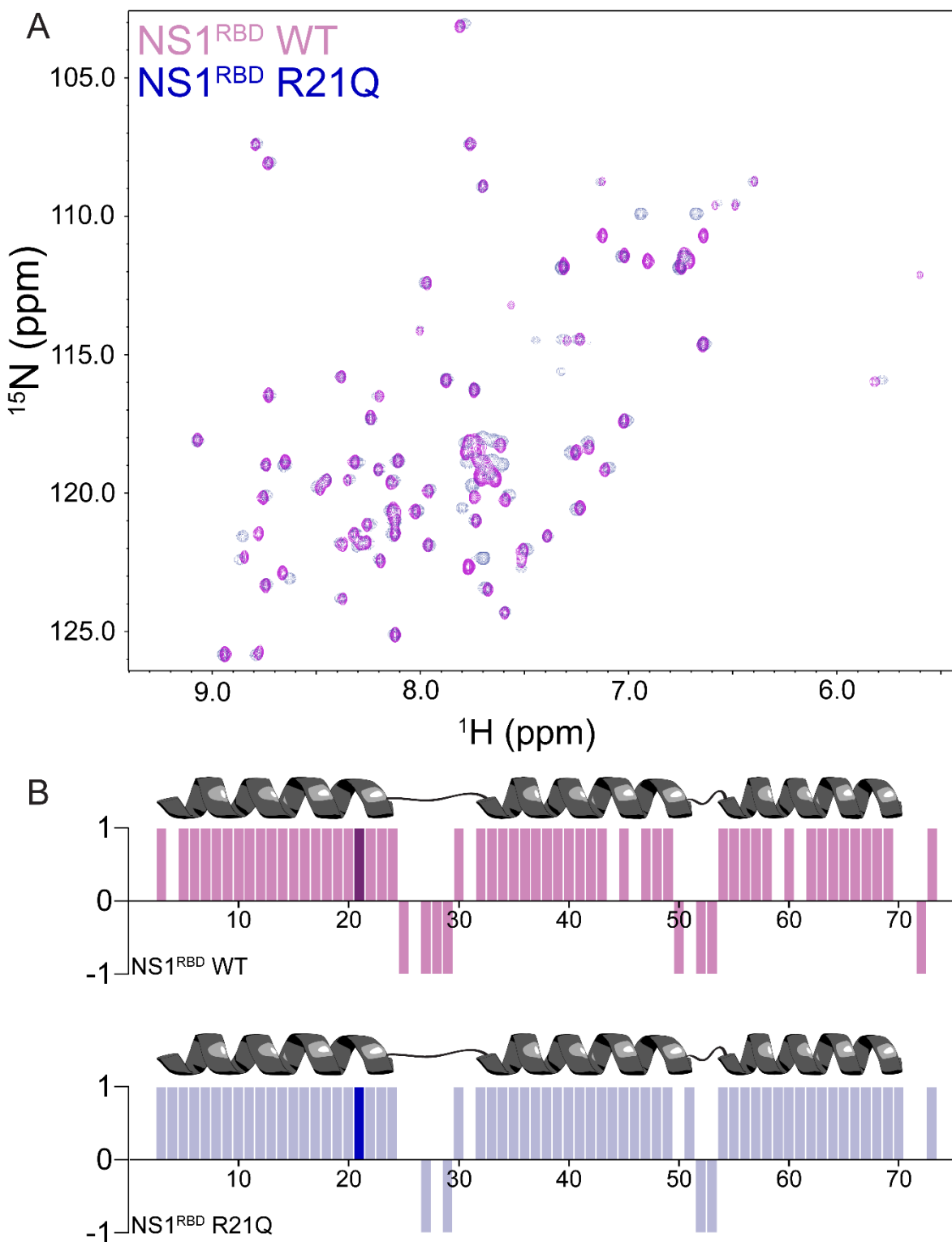


**Figure 2. The R21Q mutation has no appreciable effect on the overall structure of the NS1<sup>RBD</sup>.** (A) Overlay of the <sup>1</sup>H – <sup>15</sup>N HSQC spectra of the RBD<sup>WT</sup> (purple) and the RBD<sup>R21Q</sup> (light blue). (B) Chemical-shift index derived from <sup>13</sup>C<sub>α</sub> chemical shifts of the RBD<sup>WT</sup> (light purple) and the RBD<sup>R21Q</sup> (light blue). Position 21 is indicated by a darker shade of the color corresponding to each variant. The secondary structure is marked in each histogram using a ‘helix’ icon.



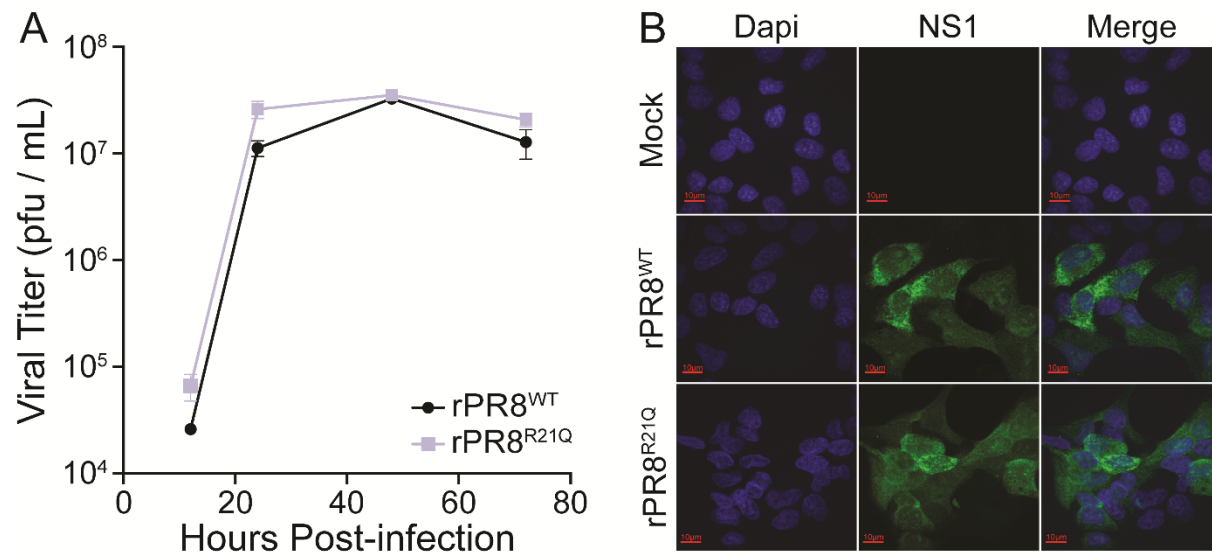


**Figure 3. Infection with rPR8<sup>WT</sup> and rPR8<sup>R21Q</sup> demonstrates similar replication kinetics and NS1 intracellular localization.** (A) A549 cells were infected with rPR8<sup>WT</sup> (black) or rPR8<sup>R21Q</sup> (lavender) at an MOI of 0.01. At 12, 24, 48, and 72 hours post-infection, supernatants were collected (n=6) and titered on MDCKs using standard plaque assays. (B) A549 cells were infected with each rPR8<sup>WT</sup> or rPR8<sup>R21Q</sup> at an MOI of 5. Cells were fixed at 12 hours post infection and stained with an anti-NS1 antibody (NS1) and DAPI (Nuclei). Localization was visualized using an Olympus FV1000 confocal microscope. Scale bars (red) signify 10  $\mu$ m.

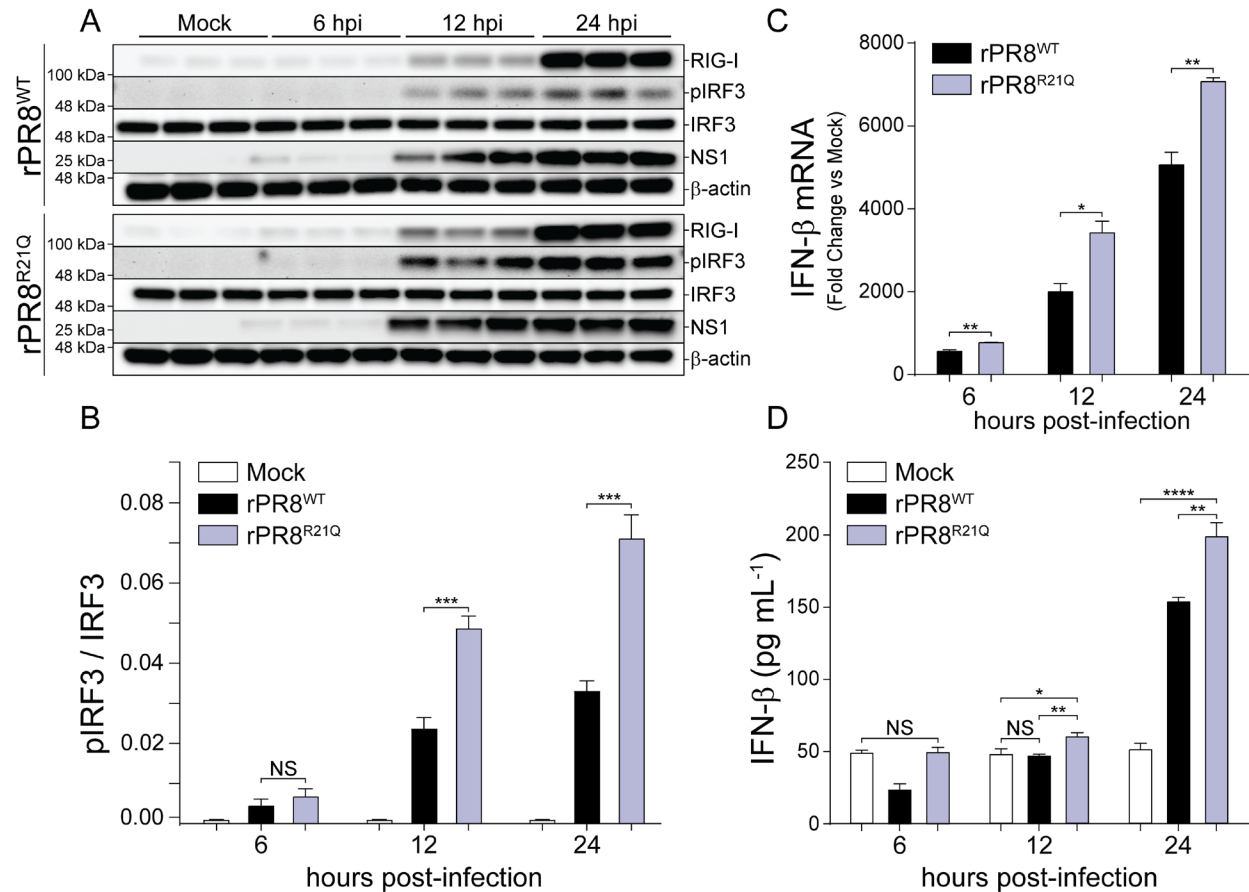


**Figure 4. Infection with rPR8<sup>R21Q</sup> results in significantly increased IRF3 phosphorylation and IFN-β expression.** (A) A549 cells were infected with rPR8<sup>WT</sup> or rPR8<sup>R21Q</sup> at an MOI of 2 for 6, 12, and 24 hours. At each respective time point, monolayers were lysed and probed by western blot for total IRF3, phosphorylated IRF3 (pIRF3), IAV NS1, RIG-I, and B-Actin. (B) The ratio of pIRF3 to IRF3 quantified in triplicate for each time point. (C) A549 cells were infected at an MOI of 2. Cell monolayers were lysed and total RNA was collected at 6, 12, and 24 hours post-infection. IFN-β mRNA expression was determined using qPCR with fold change values calculated via the  $\Delta\Delta CT$  method. (D). IFN-β levels in supernatants harvested from A549 cells infected with rPR8<sup>WT</sup> or rPR8<sup>R21Q</sup> (MOI of 2) were determined at 6, 12, and 24 hours post-infection using an IFN-β specific ELISA (manufacturer). Data were analyzed using Student's t-test and error bars represent the mean  $\pm$  standard error (\* =  $p < 0.05$ , \*\* =  $p < 0.01$ , \*\*\* =  $p < 0.001$ , and \*\*\*\* =  $p < 0.0001$ ). All data are representative of 3 independent experiments with rPR8<sup>WT</sup> indicated in black and rPR8<sup>R21Q</sup> indicated in lavender.

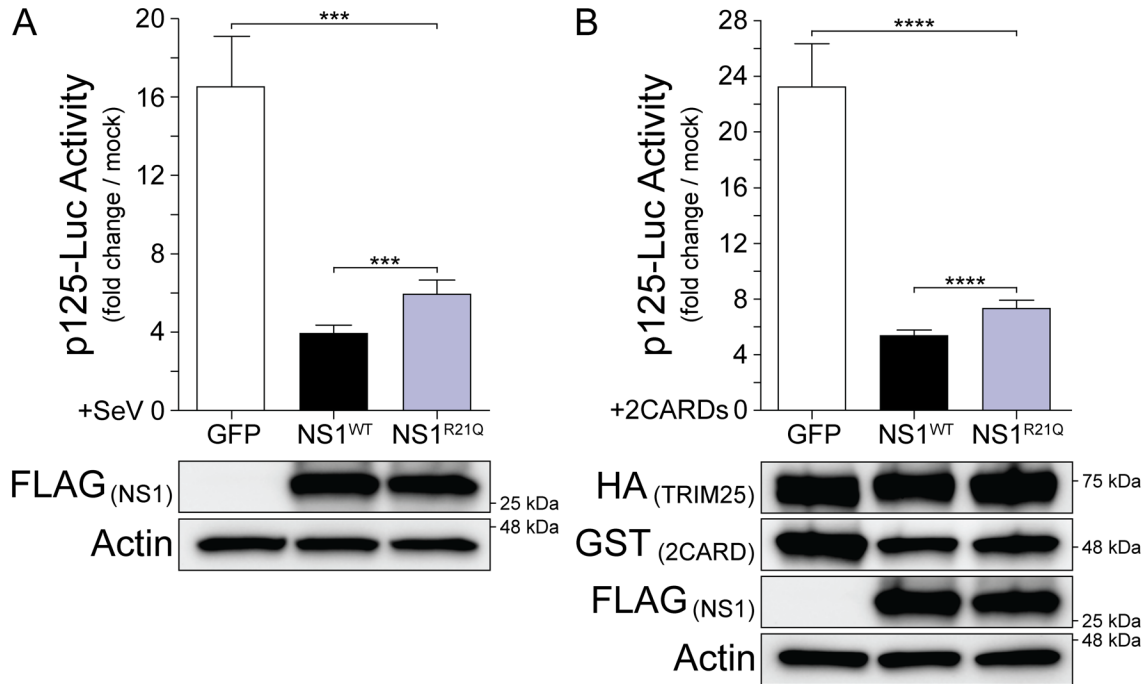


**Figure 5. NS1<sup>R21Q</sup> is less efficient at inhibition of IFN-β promoter activation.** (A) 293T cells were transfected with p125-Luc (firefly luciferase under IFN-β promoter) and pCMV-rLuc (renilla luciferase control) along with either a GFP control (white), 3xFLAG-NS1<sup>WT</sup> (black), or 3xFLAG-NS1<sup>R21Q</sup> (lavender) expression vectors. At 36 hours post transfection, cells were infected with 200 HAU of Sendai virus for 18 hours at which point IFN-β promoter activity was measured using a dual-luciferase assay (Promega). (B) 293T cells were transfected with p125-Luc, pCMV-rLuc, HA-TRIM25, and GST-2CARDs along with a GFP control (white), 3xFLAG-NS1<sup>WT</sup> (black), or 3xFLAG-NS1<sup>R21Q</sup> (lavender) expression vectors. At 24 hours, IFN-β promoter activity was measured using a dual-luciferase assay (Promega). Representative Western blots are shown to demonstrate relative transfection efficiency. All data are representative of 3 independent experiments. Densitometric analysis of expression levels of NS1<sup>WT</sup> and NS1<sup>R21Q</sup> normalized to actin expression indicate that the differences observed in both experiments are not due to differences in expression levels (data not shown). Data were analyzed using Student's t-test and error bars represent the mean ± standard error (\* = p<0.05, \*\* = p<0.01, \*\*\* = p<0.001, and \*\*\*\* = p<0.0001).

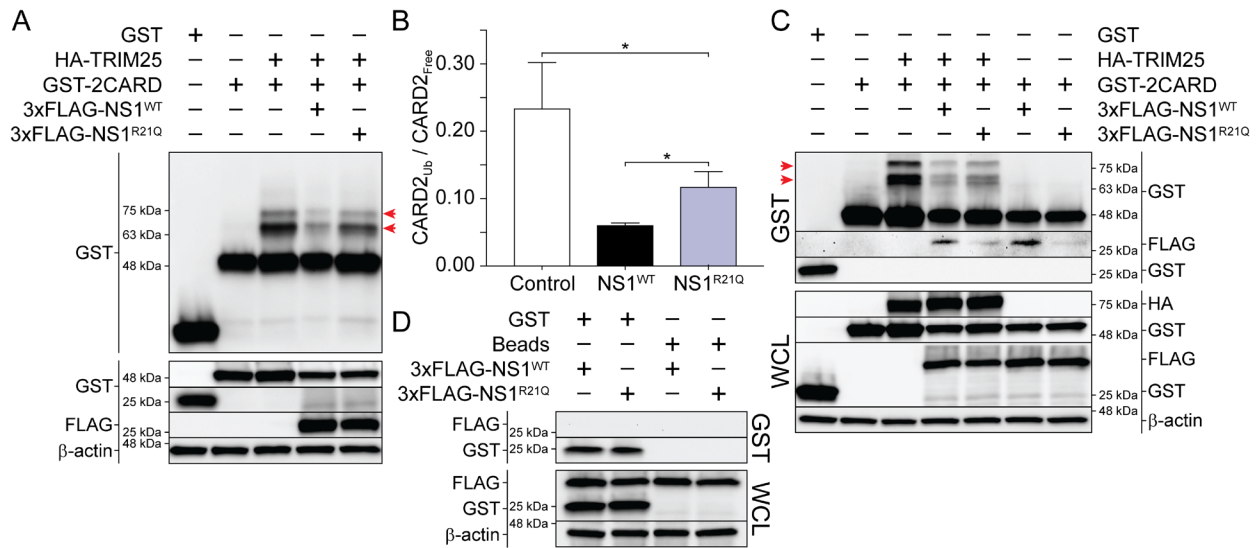


**Figure 6. NS1<sup>R21Q</sup> is less effective at inhibiting RIG-I 2CARDs ubiquitination and exhibits diminished interaction with RIG-I 2CARD.** (A) 293T cells were transfected with expression plasmids encoding the indicated combination of TRIM25, GFP (control), GST (control), RIG-I 2CARDs fused with GST (GST-2CARDs), 3xFLAG-NS1<sup>WT</sup> and 3xFLAG-NS1<sup>R21Q</sup>. At 36 hours post-transfection, GST-2CARDs was pulled down and ubiquitinated GST-2CARDs (indicated by red arrows) was visualized by western blot. (B) Densitometric analysis was used to quantify the ratio of ubiquitinated GST-2CARDs to free GST-2CARDs. NS1<sup>WT</sup> is indicated in black while NS1<sup>R21Q</sup> is indicated in lavender. (C) 293T cells were transfected with the indicated combination of expression plasmids. At 36-hours post-transfection, GST-2CARDs was pulled down and free 2CARDs, ubiquitinated 2CARDs, 3xFLAG-NS1<sup>WT</sup>, and 3xFLAG-NS1<sup>R21Q</sup> in whole cell lysates (WCL) as well as pull-down fractions were visualized by western blot. (D) 293T cells were co-transfected with either 3xFLAG-NS1<sup>WT</sup> or 3xFLAG-NS1<sup>R21Q</sup> along with a GST expression vector or GFP control. All samples were subjected to pull down with glutathione agarose and pulldown fractions were probed for 3xFLAG and analyzed by western blot.



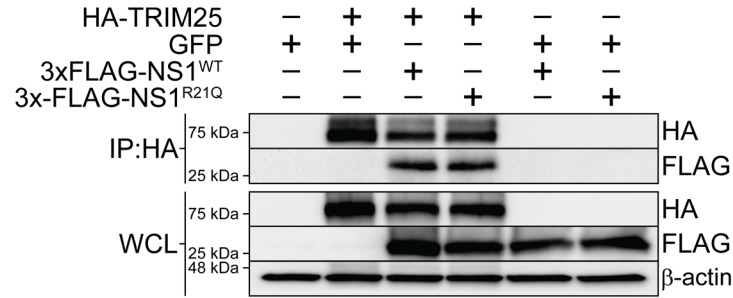


**Figure 7. The R21Q mutation has no effect on TRIM25 binding.** 293T cells were transfected with pHA-TRIM25 along with a GFP control vector, p3xFLAG-NS1<sup>WT</sup>, or p3xFLAG-NS1<sup>R21Q</sup>. 36 hours post-transfection lysates were harvested and subjected to immunoprecipitation with αHA-agarose (Pierce 26181). HA-TRIM25, 3xFLAG-NS1<sup>WT</sup>, and 3xFLAG-NS1<sup>R21Q</sup> in whole cell lysates (WCL) and immunoprecipitated fractions were visualized by western blot.

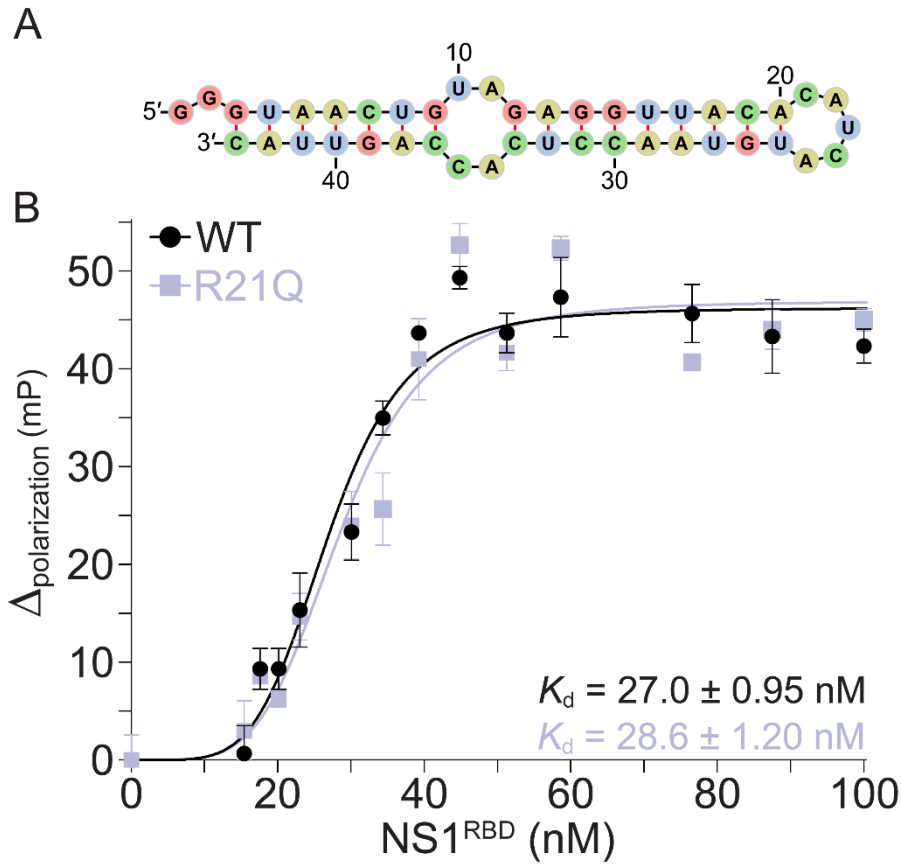


**Figure 8. The R21Q mutation has no effect on RNA binding.** (A) Graphical depiction of a previously described dsRNA structure (39) that was used to determine the effect of the R21Q mutation on the known interaction between the NS1<sup>RBD</sup> and RNA. (B). Fluorescence polarization measurements of increasing concentrations of NS1<sup>WT</sup> and NS1<sup>R21Q</sup> in the presence of 5' 6-FAM labeled shDM03 (5 nM) determined that the binding affinities of NS1<sup>WT</sup> (black) and NS1<sup>R21Q</sup> (lavender) to shDM03 were  $27 \pm 0.95$  and  $28.6 \pm 1.2$  nM respectively. Change in polarization was calculated by subtracting FP measurements of shDM03 buffer only controls from experimental FP measurements. All data are representative of three independent experiments. Error bars represent the mean  $\pm$  SEM. Binding affinities were determined by fitting data to the one-site specific binding with hill-slope (Graphpad).

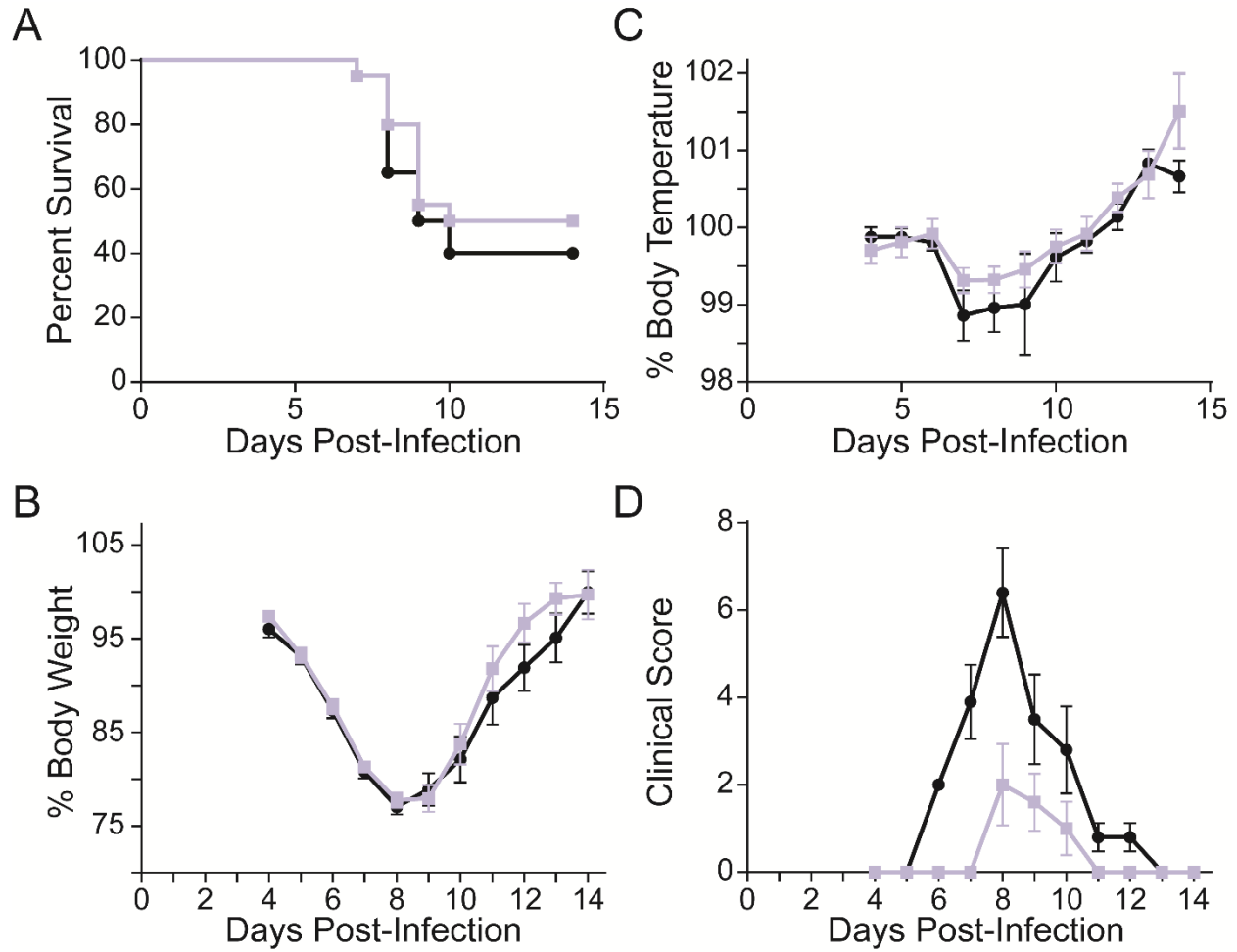


**Figure 9. *In vivo* characterization of the R21Q mutation.** Groups of 20 mice (10 female and 10 male) were inoculated intranasally with 100 plaque forming units of rPR8<sup>WT</sup> (black) and rPR8<sup>R21Q</sup> (lavender). (A) Survival, (B) weight loss, (C) temperature, and (D) clinical observations were monitored for 14 days post-infection.

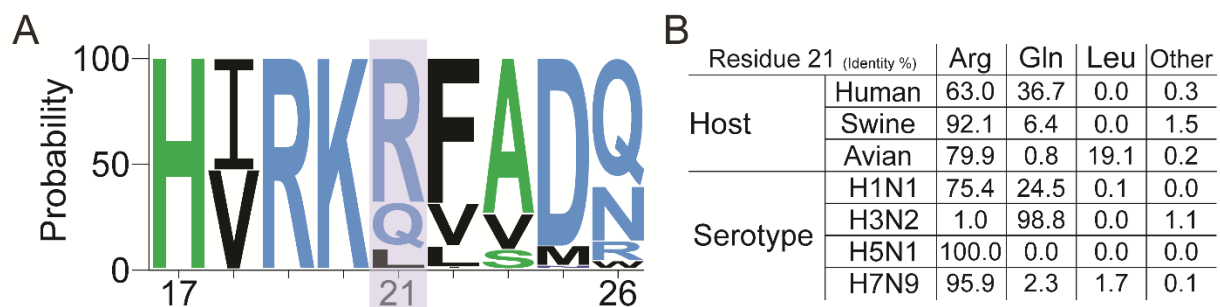


**Figure 10. Strain-specific polymorphisms at position 21 in NS1.** (A) Sequence logo describing sequence conservation at position 21 (highlighted in lavender) in NS1 (weblogo.com). (B). Percent residue identity as a function of host and serotype derived from multiple alignments of NS1 sequences obtained from the Influenza Research Database (fludb.org).



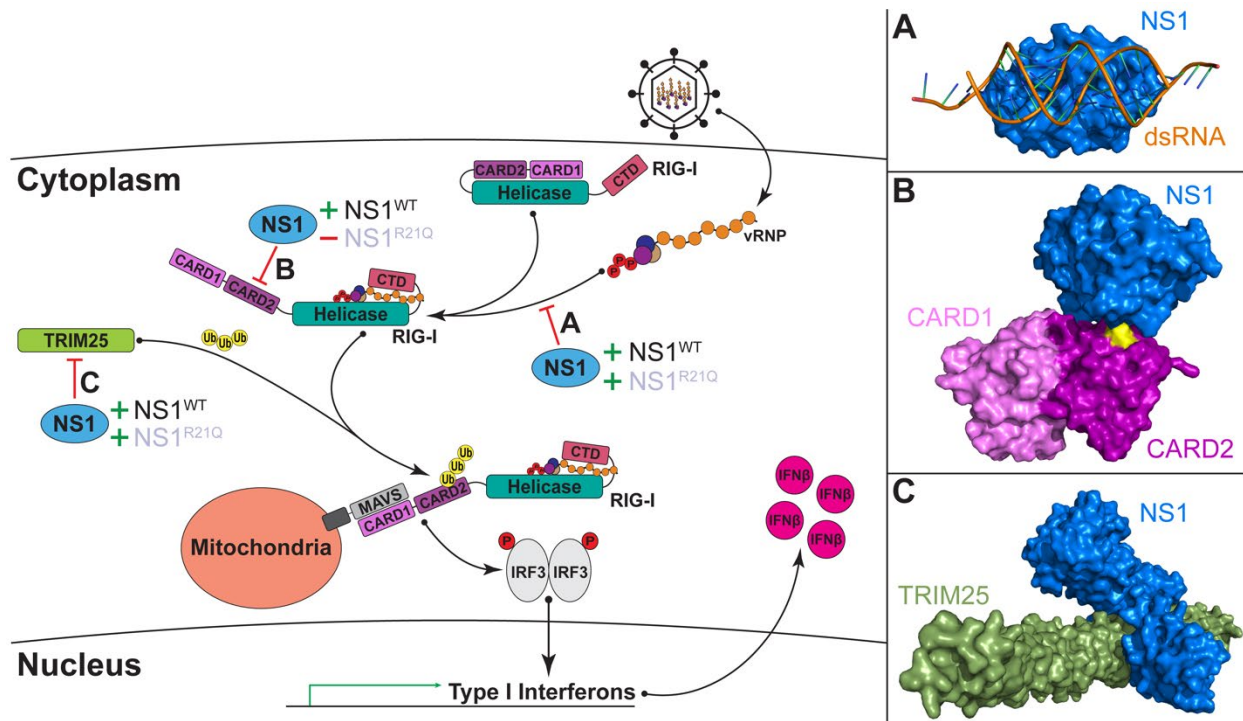


**Figure 11. Schematic representation of RIG-I activation in the context of influenza infection.** NS1 interferes with three steps in RIG-I activation which allows it to perform its overall function of antagonizing the innate immune response. The effect that the R21Q mutation has on these three specific functions of NS1 has been assessed in this manuscript. These assessments as indicated in the schematic by their respective steps in the RIG-I activation pathway. (A) NS1 is posited to antagonize RIG-I activation by shielding the presence of dsRNA structures from host proteins by directly interacting with these dsRNA structures (3). The structural basis of dsRNA recognition by NS1 of IVA is illustrated in panel A (28) (PDB: 2ZKO). As indicated in Figure 8, the R21Q mutation has no effect on the ability of the NS1<sup>RBD</sup> to bind dsRNA. (B) NS1 was previously determined to interact directly with the second CARD of RIG-I with the R21Q mutation abolishing this interaction (8). Additional data presented in this manuscript supports this observation (Figure 6C) and indicates that the R21Q mutation also reduces NS1's ability to inhibit ubiquitination of 2CARDS (Figure 6A and B). A hypothetical model of the interaction between the NS1<sup>RBD</sup> and CARD2 is illustrated in panel B using previously solved structures of 2CARDS (PDB: 4NQK) (49) and the NS1<sup>RBD</sup> (PDB: 2N74) (8). The most critical position of 2CARDS ubiquitination (K172) is indicated in yellow. (C) TRIM25 is the E3-ubiquitin ligase that is responsible for K63-specific polyubiquitination of 2CARDS of RIG-I at position K172. NS1 interacts directly with TRIM25 to inhibit RIG-I ubiquitination thereby suppressing activation of the RIG-I pathway (38). The structural basis of NS1-mediated TRIM25 (PDB: 5NT2) inhibition is illustrated in panel C. As indicated in Figure 7, the R21Q mutation does not abolish the interaction between NS1 and TRIM25.

**The influenza NS1 protein modulates RIG-I activation via a strain-specific direct interaction with the second CARD of RIG-I**

Alexander S. Jureka, Alex B. Kleinpeter, Jennifer L Tipper, Kevin S Harrod and Chad M. Petit

*J. Biol. Chem.* published online December 16, 2019

---

Access the most updated version of this article at doi: [10.1074/jbc.RA119.011410](https://doi.org/10.1074/jbc.RA119.011410)

Alerts:

- [When this article is cited](#)
- [When a correction for this article is posted](#)

[Click here](#) to choose from all of JBC's e-mail alerts